Luminescence of Intraporous Cerium(III) Complexes in Alkyl Sulfonic Mesoporous Silica

K. Klier,*,† A. C. Miller,‡ L. L. Zhang,†,§ and M. K. Hatalis⊥

Department of Chemistry, The Scienta Laboratory of the Materials Research Center, Undergraduate Pool Foundation Fellow, Department of Electrical and Computer Engineering and Flexible Displays Lab of the Center for Optical Technologies, Lehigh University, Bethlehem, Pennsylvania 18015

Received July 3, 2007. Revised Manuscript Received November 19, 2007

Mesoporous silica materials derivatized with propyl-sulfonic groups (SBA-15) with a monovalent cation-exchange capacity of ~1 meq/g were exchanged with Ce(III) ions to ~0.5 meq/g to form Ce(III)SBA material displaying high-intensity purple photoluminescence. XPS and NIR-DRS analysis suggests the Ce(III) ion is bound to two proximal propyl-sulfonate groups and capped with a hydroxyl in a complex $[\equiv Si-(CH_2)_3SO_3]_2Ce(III)OH \cdot xH_2O$ ($x > 4$), where the coordinated water can be almost completely removed by anoxic dehydration at 350 C to $x < 0.2$. The white hydrated ($x \geq 4$) CeSBA and the brown-colored dehydrated ($x < 0.2$) CeSBA exhibit fluorescence with comparable integrated intensities at 368 and 394 nm, respectively. The Ce(III) 4f electron is located by XPS above the top of the Si 3p O 2p valence band, thus identifying the Ce(III) 4f orbital as the HOMO. Photoluminescence emission and excitation spectra of the 5d → 4f transition display Stokes shifts and structure sensitivity consistent with a direct transition process not involving, in these SBA materials, a multistep energy transfer previously invoked for oxide cerium-containing phosphors. A quantitative assessment of the relaxation was made on the basis of calculation of vibrational frequencies in DFT-optimized structures of a disulfonate−La−OH species with and without additional coordinated water.

Introduction

Trivalent rare-earth (RE) phosphors are widely used in practical applications involving lighting, lasers, and detectors of many forms of radiation. The present research is motivated by the potential of various RE-containing inorganic and organic complexes and compounds as viable components of LED displays, including our continuing research effort in fabrication of flexible displays.[1] As an attractive alternative to synthetic incorporation of RE into inorganic phosphors or metal-organic complexes, ion-exchanging materials provide for an easy control of concentration, are amenable to multiple RE ion-exchange, and as demonstrated in this report, exhibit chemical and optical stability in the hydrated state. In addition, mesoporous ion-exchanging materials contain channels available for incorporation of semiconducting inorganic or organic "molecular wires" that can be used with advantage in the design of electroluminescent components of LED devices.

In this communication, we report on the preparation, stoichiometry, electronic structure, and optical properties of rare-earth (RE) hybrid organic-silicaceous materials in terms of binding, valence band (VB) structure, and photoluminescence (PL) of Ce(III) exchanged into a mesoporous silica, the SBA-15 material, that is derivatized with intraporous alkyl-sulfonic groups[2] and possesses a high ion-exchange capacity.[3] The stoichiometry is determined by a combination of quantitative core-level XPS and near-infrared spectroscopy to yield isostructural $-[\text{alkyl-}SO_3]_2RE(III)OH$ complexes in which the different RE(III) ions display a variety of luminescence colors. The high surface concentration of the sulfonic groups affords proximal sites that are essential for the formation of the RE(III) complexes. High-resolution VB-XPS reveals supravalence 4f levels as a HOMO source for excitations within an $-[\text{alkyl-}SO_3]_2Ce(III)OH$ complex that are localized on the Ce(III) cations, configuration $[Xe]4f^1$ and are absent in La(III), $[Xe]4f^0$. We also present full-potential linearized plane-wave DFT calculations on the optimized structures, which correctly account for the VB electronic structure, including the location of the Ce(III) 4f electron above the top of the VB.

Of general interest are not only optical but also catalytic and sorption applications of the RE−SBA materials. Previous communications from this laboratory established the surface ratio of alkyl-sulfonic groups to the Si atoms in the silica "wall" 1:7,[3] which enabled a unique catalytic mechanism for dehydrocondensation of alcohols to unsymmetrical ethers over the acid form of the SBA material

* Corresponding author. E-mail: kk04@lehigh.edu.
† Department of Chemistry, Lehigh University.
‡ The Scienta Laboratory of the Materials Research Center, Lehigh University.
§ Undergraduate Pool Foundation Fellow, Lehigh University.
⊥ Department of Electrical and Computer Engineering and Flexible Displays Lab of the Center for Optical Technologies, Lehigh University.

(1) Chuang, T.-K.; Troccoli, M.; Kuo, P.-C.; Jamshidi, A.; Spirko, J. A.; Hatalis, M. K.; Klier, K.; Biaggio, I.; Voutsas, A. T.; Afentakis, T.; Hartzell, J. W. *Electrochem. Soc. Trans.* **2006**, *3*, 349 "Thin Film Transistor Technology".

(2) (a) Melero, J. A.; Stucky, G. D.; Grieken, R. Van; Morales, G. *J. Mat Chem* **2002**, *12*, 1664. (b) Margolese, D.; Melero, J. A.; Christiansen, S. C.; Chmelka, B. F.; Stucky, G. D. *Chem. Mater.* **2000**, *12*, 2448.

(3) Shen, J. G. C.; Herman, R. G.; Klier, K. *J. Phys. Chem. B* **2002**, *106*, 9975.

10.1021/cm071754g CCC: $40.75
Published on Web 01/04/2008

by the dual-site surface S_N2 mechanism.[4] This mechanism requires flexible proximal alkyl-sulfonic sites and the mesoporous material provides accessibility to large molecules. The sulfonic groups have also been proven to be specific sites for binding nitrogen bases of variable strength that correlated with the S2p and N1s XPS core-level shifts and were accounted for by theoretical calculations.[5] Furthermore, proximity of the sulfonic groups has proven to be essential for near-stoichiometric binding of Me(II) ions. Although the high surface concentration of the tethered alkyl-sulfonic groups was established for dual-site catalysis and binding of Me(II) ions, the ability of these materials to bind the trivalent RE(III) ions was by no means obvious because of the requirements to utilize three sulfonic moieties or capture another anion from the solution during the preparation.

Although there are a number of literature reports on luminescence of transition-metal[6,7] and rare-earth metal ions in zeolites,[8,9] the more recently discovered mesoporous materials have not been investigated to any comparable extent in regard to photo and electroluminescence. To the best of our knowledge, Ce(III) ions have been introduced only into a non-ion-exchanging mesoporous silica by "soaking" with a Ce(IV) salt followed by a partial self-reduction to Ce(III), while impregnation by a Ce(III) salt has not yielded detectable luminescence because of too small concentrations of the luminophor achieved by this method.[10] In contrast, using the present SBA material with a high proton-exchange capacity of the $-SO_3H$ groups, we have found an easily achievable complete exchange with the Ce(III) ions from aqueous chlorides with no occlusion of the anion. The resulting material, Ce(III)−SBA, displays a strong purple luminescence. We have also examined the effect of water on the luminescence and other properties of this material as a function of dehydration conditions. Combined with the recently reported synthesis of thin, oriented overlayers of mesoporous silicas interfaced with flat supports,[11] these materials afford a great many design options for a variety of applications in interface chemistry and optoelectronics.

Experimental Section

Materials and Procedures. The mesoporous SBA-15 material was synthesized at 313K from tetraethoxysilane (TEOS) and 3-mercaptopropyltrimethoxysilane (MPTMS) with Pluronic 123 $EO_{20}PO_{70}EO_{20}$ triblock copolymer (MW = 5800, Aldrich) as the templating agent using the one-step direct synthesis procedure of Margolese et al.[2] and as described previously in reports from this laboratory.[3–5] The efficiency of the Pluronic removal by a 24 h ethanol reflux and the completeness of oxidation of the mercaptopropyl to propyl sulfonic groups was checked by XPS analysis as described below.

The ion-exchange with Ce(III) was carried out with 0.5 g of the room-temperature dried SBA-15 material with 100 mL of ca. 0.1 M aqueous solution of 99.99% $CeCl_3.7H_2O$ (Alfa Aesar) at 29 °C for 3 h, filtered on Whatman 2, and washed with copious amounts of distilled water. A subsequent thermal treatment of the samples included an overnight drying at 60 °C in air and a dehydration at 350 °C under argon for 1 h. Each of the preparations, room-temperature dried, 60 °C dried, and 350 °C dehydrated, was subject to the XPS, NIR, VISUV, and PL spectroscopic measurements outlined below. The results reported here concern only the 60 °C dried and 350 °C dehydrated samples, because the room-temperature dried sample contained an undefined amount of water and displayed the same luminescence parameters as the 60 °C dried sample.

XPS Analysis. High-resolution XPS analyses, recording the Ce 3d, Ce 5p, S 2p, O 1s, Si 2p, Si 2s, C 1s, Cl 1s, and valence band spectral regions, were carried out using the Scienta ESCA-300 spectrometer.[12] An electron flood gun was used to neutralize charging of the insulating samples, as in our earlier work.[5] The Si 2p binding energy (BE) of 103.5 eV was used as an internal standard for all peak positions. For a quantitative analysis, the Scienta-300 sensitivity factors relative to C1s (RSF) were those of Hunsicker et al.[13] for Si 2p (1.13), O 1s (2.84), Johansson et al.[14] for S 2p (1.68), and in addition RSF = 30.5 for the Ce $3d_{5/2}$ emissions. The S 2p emissions of all the SBA materials were overlapping $2p_{3/2}$ and $2p_{1/2}$ peaks and were integrated over the 2p region separately for the oxidized sulfur of the $-SO_3$ groups with S 2p at 167.1 eV and the unoxidized −SH with S2p at 162.2 eV. Under these conditions, previous XPS analyses of the SBA-15 material exchanged with various cations have shown to account for bulk composition to within relative 15 at %.[15] After a complete removal of the Pluronic copolymer and oxidation of the thiol groups of the precursor MPTMS by H_2O_2, most of the sulfur was in the oxidized state, corresponding to the composition of the pendant $-(CH_2)_3-SO_3H$ groups, with a small amount (<5%) of the unoxidized thiol $-(CH_2)_3-SH$. The stoichiometry of the Ce-containing materials was verified by XPS analysis by referencing to a commercially available Ce(III) triflate (Alfa Aesar stock L20251, lot USLF004818, CAS 76089–77–5, 98% purity), which yielded the ratios S:Ce = 2.86, C:S = 0.96, and F:C = 2.77. In particular, the S:Ce ratio obtained by using the above RSFs was to within relative 5% of the theoretical 3.0.

Near-Infrared Reflectance (NIR) Spectroscopy for Water, Hydroxyls, and C−H Groups. The NIR region between 4500 and 10 000 cm^{-1} was used primarily for the detection and analysis of water and hydroxyls at various stages of ion-exchange and dehydration of the SBA material. The Cary 500 spectrophotometer was equipped with a diffuse reflectance (DRS) attachment with a PbSe NIR detector at the periphery of the Halon-coated integration sphere. The Halon standard was also used as a reference, and

(4) Hasan, S. S.; Herman, R. G.; Klier, K. In *Molecular Sieves: From Basic Research to Industrial Applications*; Studies in Surface Science and Catalysis; Čejka, J., Žilková, N., Nachtigall, P., Eds.; Elsevier: Amsterdam, 2005; Vol. 158B, p 1343.
(5) Smith, J. L.; Herman, R. G.; Terenna, C. R.; Galler, M. R.; Klier, K. *J. Phys. Chem. A* **2004**, *108*, 39.
(6) Strome, D. H.; Klier, K. *J. Phys. Chem.* **1980**, *84*, 981.
(7) Klier, K. *Langmuir* **1988**, *4*, 13–25.
(8) Tanguay, J. F.; Suib, S. L. *Catal. Rev.−Sci. Eng.* **1987**, *29*, 1.
(9) Jüstel, T.; Wiechert, D. U.; Lau, C.; Sendor, D.; Kynast, U. *Adv. Funct. Mater.* **2001**, *11*, 105.
(10) Cai, W.; Zhang, Y.; Zhang, L. *J. Phys.: Condens. Matter* **1998**, *10*, L473.
(11) Hussen, G. N. A.; Shirakawa, H.; Nix, W. D.; Clemens, B. M. *J. Appl. Phys.* **2006**, *100*, 114322.
(12) Gelius, U.; Wannberg, B.; Baltzer, P.; Fellner-Feldegg, H.; Carlsson, G.; Johansson, C.-G.; Larsson, J.; Münger, P.; Vegerfors, G *J. Electron Spectrosc. Relat. Phenom.* **1990**, *52*, 747.
(13) Hunsicker, R. A.; Klier, K.; Gaffney, T. S.; Kirner, J. C. *Chem. Mater.* **2002**, *14*, 4807.
(14) Johansson, M. Ph.D. Thesis, Lehigh University, Bethlehem, PA, 1995.
(15) Smith, J. L.; Herman, R. G.; Klier, K. In *Molecular Sieves: From Basic Research to Industrial Applications*; Studies in Surface Science and Catalysis; Čejka, J., Žilková, N, Nachtigall, P., Ed.; Elsevier: Amsterdam, 2005; Vol. 158A, p 797.

corrections to the Schuster−Kubelka–Munk (SKM) for the ratio of absorption and scattering coefficients based on the albedo of isotropic scattering in turbid media were made following the procedure outlined by the author.[16]

The NIR analysis of various states of hydrogen bonding and agglomeration of intraporous water and hydroxyls involves overtone and combination bands $H_2O(\nu + \delta)$ near 5000 cm^{-1}, $H_2O(2\nu)$ near 6800 cm^{-1}, and $-OH(2\nu)$ near 7300 cm^{-1}. These bands are due to transitions (000) → (011) and (000) → (101) for water, where (v_1 v_2 v_3) are the vibrational quantum numbers of the symmetric stretching (ν_1), bending (v_2), and antisymmetric stretching (v_3) modes, and to transition 0 → 2 for the stretching mode of the hydroxyls. The state of bonding, agglomeration, interaction, and dynamical motion of these species is reflected in the band center positions, line widths, and shapes. The water bands near 5000 cm^{-1} involving the bending mode ν_2 are absent if all the OH vibrations are due to hydroxyls only. In addition, the C−H overtones around 5600–5900 cm^{-1} are detected in the present system because of the presence of the propyl links between the silica "wall" and the ion-exchanging $-SO_3H$ groups.

The SBA samples, after various treatments that included dehydrations at elevated temperature under argon, were placed in the DRS cell provided with a Suprasil window without exposure to air.

Visible and UV Diffuse Reflectance Spectroscopy (Vis−UV−DRS) for the Band-to-Band and Charge-Transfer Transitions. The Vis−UV region covered the range 10 000–45 000 cm^{-1} and was recorded in the same experimental setup as the NIR-DRS, except a red-sensitive photomultiplier was used at the periphery of the integration sphere.

Photoluminescence (PL) Spectroscopy. The PL spectra were recorded using the Cary Eclipse spectrometer, using the solid-state powder DRS cell supplied by the manufacturer provided with a 0.5 mm thick quartz window and a screw-hand press to achieve compact consistency of the powders. The PL intensity of the hydrated, 60 °C dried, and 350 °C dehydrated CeSBA samples was visible as a purple emission under illumination by the UVP UVG-54 short-wave 254 nm lamp. Moreover, integrated intensities of the PL were comparable for all three preparations. Quantum efficiency was not determined because of lack of data on the scattering power of the SBA material. The emission and excitation spectra were obtained by scanning the exit or entry monochromator and using filters to block spurious signals or higher order reflections. The wavelength range of this spectrometer covers 190–1100 nm and the broadpass filter ranges are 295–1100, 360–1100, 430–1100, and 550–1100 nm. The slitwidths were 10 nm for each of the monochromators.

Results and Discussion

XPS Analysis, Identification of Valence States, and Stoichiometry. As in our earlier study of the same SBA preparation, the C:S ratio was near the expected value 3:1 after the removal of the Pluronic, and exchangeable proton concentration was ∼1 meq/g,[3,5] on the basis of integrated areas of the C1s and S2p peaks with subtracted linear backgrounds divided by RSF. After exchange with Ce(III) chloride, XPS analysis revealed no detectable Cl, more than 95% of the sulfur in oxidized state as evidenced by the binding energy of S 2p at 167.2–167.8 eV, and some residual thiol sulfur S 2p at 161.5–162.4 eV at <5%. All Ce emissions were characteristic of the trivalent state Ce(III). The Ce(III) $3d_{5/2}$ and $3d_{3/2}$ peaks had maxima at 884.6 and 903.0 eV. On the basis of integrated areas of the S2p and Ce$3d_{5/2}$ peaks with subtracted linear backgrounds and divided by RSF, we found the atomic ratio to be S:Ce = 2.13 in the sample dried at 60 °C, labeled CeSBA-60, consistent with the stoichiometry S:Ce = 2:1 to within relative 7%. This stoichiometry indicates that in addition to the two monovalent $-SO_3^-$ groups, the Ce(III) ion would require another anion. In the absence of Cl^-, this stoichiometry suggests a coordinated hydroxyl, as summarized by the equation

$$2 \equiv Si-(CH_2)_3SO_3H + CeCl_3(aq) + H_2O \rightarrow [\equiv Si-(CH_2)_3SO_3]_2Ce(III)OH{\cdot}xH_2O + 3HCl\,(aq) \quad (1)$$

The Ce surface complex formed in this way requires two proximal sulfonic sites, which is ensured by the high surface concentration of the propyl-sulfonic functionalities, ca. one $-(CH_2)_3SO_3^-$ group per 7 Si atoms on the intrapore silica wall.[3,5] In principle, the observed average composition can be realized by a mixture of three-coordinated hydroxyl-free sites $[\equiv Si-(CH_2)_3SO_3]_3Ce{\cdot}xH_2O$ and dihydroxylated sites $[\equiv Si-(CH_2)_3SO_3]Ce(OH)_2{\cdot}xH_2O$, but such a possibility is unlikely because of low probability of three proximal sulfonic functionalities and an accidental equimolarity of the three-coordinated and the dihydroxylated sites. Upon anoxic dehydration at 350 °C, the sample labeled Ce(III)SBA-350 showed a loss of water and some redistribution of Ce and S, but the appearance of Ce XPS peaks remained unchanged except for a small shift to lower BEs upon dehydration, exemplified in Figure 1 for Ce $3d_{5/2}$ emissions, indicating the same valence state and similar chemical environment of Ce in Ce(III)SBA-60 and Ce(III)SBA-350.

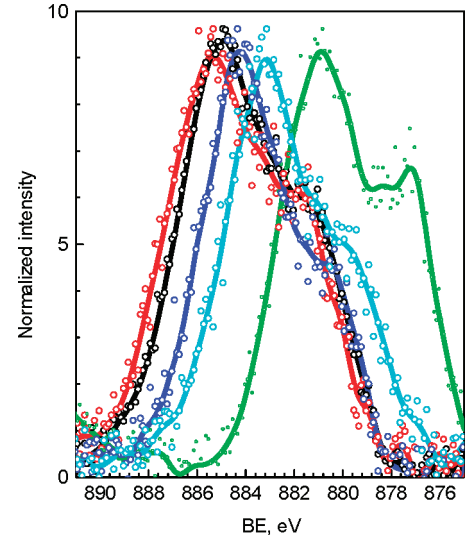

Figure 1. XPS Ce $3d_{5/2}$ core-level bands of Ce(III)SBA-60 (red), Ce(III) SBA-350 (black), and Ce(III) exchanged into commercial polyelectrolytes, hydrocarbon polystyrene sulfonates Amberlite (blue), Biorad (cyan), and fluorosulfonate Nafion (green). The XPS spectra were acquired under identical conditions. The core-level shifts (CLS) of binding energies (BE) and lineshapes are sensitive to chemical environment even for related hydrocarbon-sulfonates. However, the present Ce(III)SBA CLS and lineshapes remained unchanged upon loss of water by dehydration.

(16) Klier, K. In *Spectroscopic Studies of Zeolites and Mesoporous Materials* Studies in Surface Science and Catalysis; Čejka J., van Bekkum, H., Eds.; Elsevier: Amsterdam, 2005, Vol. 157, p 205.

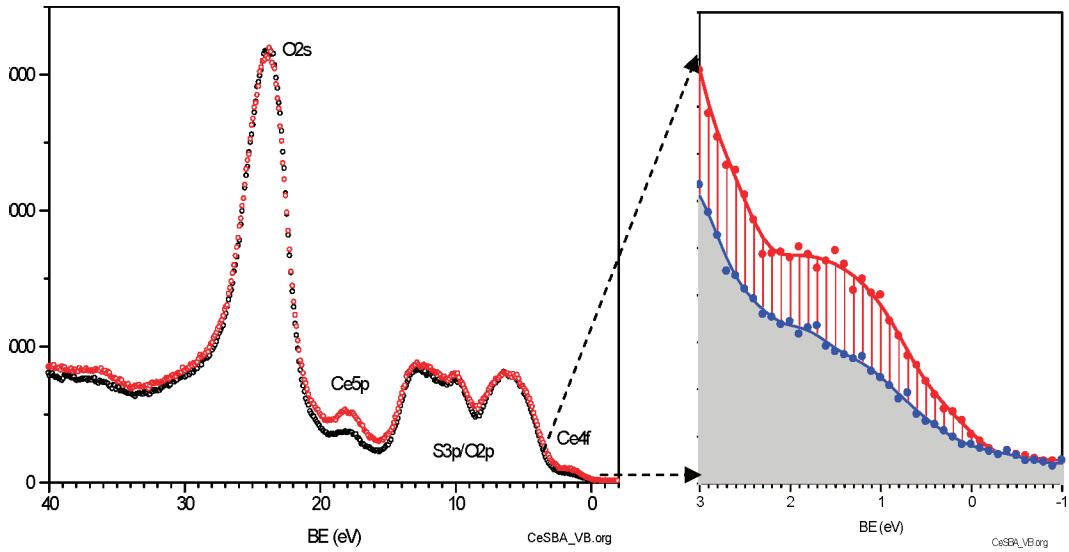

Figure 2. Valence band of Ce(III)SBA-60 (red) and Ce(III)SBA-350 (blue) showing the sub-VB Ce 5p and Ce 4f XPS levels. The DFT-FPLAPW calculations (see the Supporting Information) are in a complete agreement with the single 4f electron occupancy localized at Ce(III) some 2 eV above the top of VB.

Although the above XPS analyses are based on a quantitative measurement of the core-level emissions, additional interesting qualitative features are observed in the valence-band (VB) region, cf. Figure 2.

Here the unique feature is the Ce4f emission at the top of the O 2p/S 3p VB, identifying the single 4f electron of Ce(III) as a HOMO. Another XPS emission of Ce(III) is that of Ce 5p at BE 18 eV between the bottom of the VB and O 2s at BE 25 eV. The spectra of the Ce(III)SBA-60 and Ce(III) SBA-350 samples show a loss of some 50% of Ce(III) 4f, Ce 5p, and even Ce 5s intensity upon heating at 350 °C. This loss of XPS intensity is attributed to a migration of the Ce ions into subsurface regions. At the same time, Ce remains in the system as a trivalent species because the material still exhibits luminescence characteristic of Ce(III) as demonstrated below. No new Ce(IV) emissions are observed in the Ce 3d region. The XPS analysis of the S 2p emissions also shows corresponding loss of intensity, indicating redistribution of the —SO_3^-Ce species into preferential location in the bulk of the material. In addition, the 350 °C heated SBA material turns visibly brown, whether or not exchanged with Ce. These results indicate some degradation of chemical stability of the SBA material upon temperature treatment of 350 °C, at variance with the original indications.[2] On the contrary, the white Ce-exchanged SBA-60 is a well-defined compound of stoichiometry described by eq 1 with >95% of sulfur in the oxidized state. Nevertheless, the Ce(III) species remain centers of intense luminescence in both Ce(III)SBA-60 and Ce(III)SBA-350, as shown in detail in the section on fluorescence.

Hydroxyls and Water. To determine the state of hydration and hydroxylation, we used NIR reflectance spectroscopy to detect vibrational overtones and combination bands of Ce(III)SBA-60 and Ce(III)SBA-350 between 4500 and 8000 cm^{-1}, as shown in Figure 3.

The Ce(III)SBA-60 material reveals a significant amount of hydration and adsorbed water: the broad $H_2O(\nu+\delta)$ band near 5200 cm^{-1} indicates substantial agglomeration into

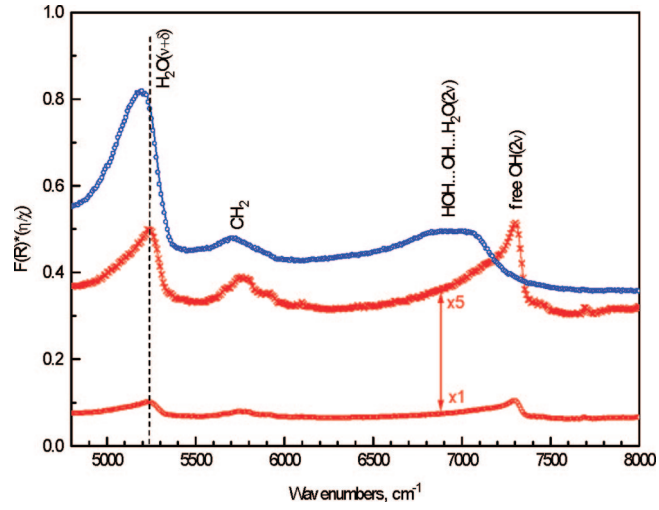

Figure 3. NIR spectra of Ce(III)SBA-60 (blue) and Ce(III)SBA-350 (red) showing the loss of water and evolution of free hydroxyls upon anoxic dehydration at 350 C.

hydrogen-bonded clusters, and the water-hydroxyl band at 6800–7200 cm^{-1}, denoted as $[HOH\cdots OH\cdots OH_2](2\nu)$ in Ce(III)SBA-60, indicates the presence of both molecular water and hydrogen-bonded hydroxyls, because its large width and shape are significantly different from molecular water only.[17] The overtones of the propyl groups are labeled as CH_2.

Upon dehydration at 350 °C, the $H_2O(\nu+\delta)$ band near 5200 cm^{-1} shows a substantial albeit incomplete loss of water, its shift to higher frequency indicates less hydrogen bonding, and the frequency of the OH(2ν) band at 7300 cm^{-1} shows that these are free OH groups, associated with only a small amount of water that appears as a lower frequency shoulder. Because the $H_2O(\nu+\delta)$ bands are roughly five times as intense as the 2ν bands,[17] we estimate the amount of residual water in Ce(III)SBA-350 to be considerably smaller than that of the hydroxyls. The OH(2ν) band with a

(17) Klier, K.; Shen, J. H.; Zettlemoyer, A. C. *J. Phys. Chem.* **1973**, *77*, 1458.

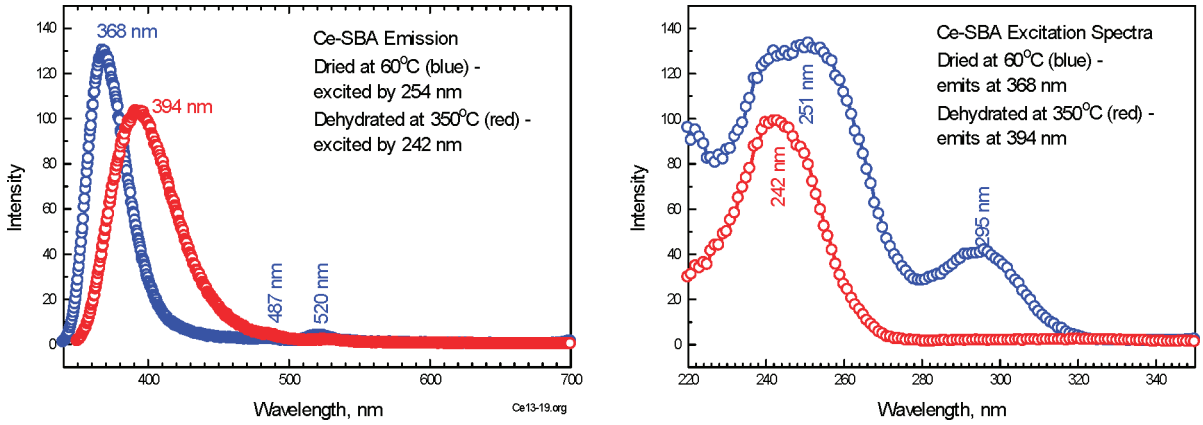

Figure 4. Luminescence spectra of Ce(III)SBA-60 (blue) and Ce(III)SBA-350 (red): (a) emission, (b) excitation.

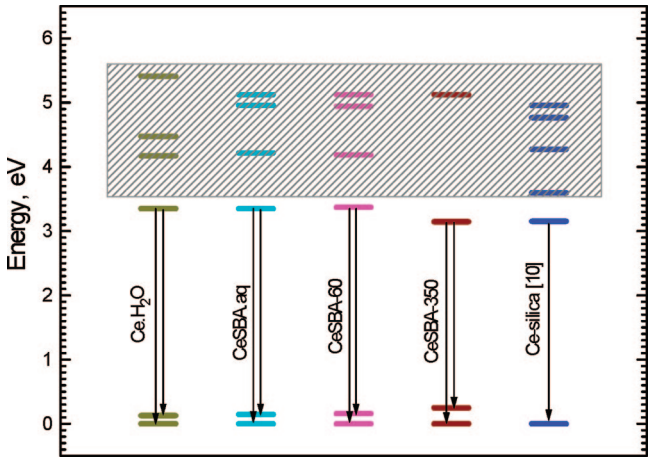

Figure 5. Luminescence spectra of Ce(III) (aq), Ce(III)SBA (aq), Ce(III) SBA-60, Ce(III)SBA-350, and Ce−silica from ref 10. Shaded area includes centers of excitation Ce4f → Ce5d bands, below which are depicted the Ce5d → Ce4f emissions from the relaxed Ce 5d geometry. The lower 4f doublets are obtained by resolution of the asymmetric down-transitions to two Gaussians.

maximum at 7300 cm^{-1} can be attributed to the cerium complex $[\equiv Si-(CH_2)_3SO_3]_2Ce(III)OH\cdot xH_2O$ formed by reaction 1 with $x < 0.2$, or to some other hydroxylated species in the system, including silanols. Because of unchanged CLS of Ce3d upon dehydration, the OH bonding to Ce(III) is more likely and remains unaffected by the number x of the weakly coordinated water molecules.

Fluorescence. UV-stimulated photoemission was observed with both the Ce(III)SBA-60 and the Ce(III)SBA-350 samples as asymmetric bands at 368 and 394 nm, respectively, as shown in Figure 4a. The corresponding excitation spectra are shown in Figure 4b.

Integrated emission intensities of the two samples excited by the short UV wavelengths are comparable, and in addition, the near-UV 295 nm excitation of Ce(III)SBA-60 gives rise to the same 368 nm emission band with proportionally decreased intensity. Both samples display large Stokes shifts, 0.8–1.75 eV for Ce(III)SBA-60 and 1.98 eV for Ce(III)SBA-350. These features show structure-sensitivity to the coordination and site geometry that is attributed to the excited state 5d, as the XPS data indicate a lack thereof for the ground state 4f.

We shall examine the origin of the Stokes shifts and their differences between the hydrated and dehydrated Ce(III)SBA materials. In earlier models, Ce(III) luminescence in various oxide phosphors has been interpreted as a multistep process because of the excitation of the 4f electron into local or delocalized UV states followed by excitation energy transfer to crystal-field split Ce(III) 5d states and subsequent emission 5d → 4f.[9,18] The present results, however, are consistent with a simpler direct mechanism that does not involve intermediate excitation energy transfer through a solid oxide matrix. Herein, we present a semiquantitative account of the observed large Stokes shifts on the basis of a calculation of vibrational frequencies of the RE−OH and $RE(H_2O)_4OH$ modes in the model disulfonic-hydroxyl complexes.

Water-Free Ce(III)SBA. The fluorescence behavior is exemplified by the Ce(III)SBA-350 spectra, where the Stokes shift is the largest. The geometry for the Franck–Condon excitation 4f → 5d is that of the ground state, and the Ce. . .OH distance, 0.2122 nm, is close to the calculated optimized La···OH distance, d(La−OH) = 0.2105 nm (see the Supporting Information). This result is consistent with the close values of ionic radii of La(III) and Ce(III), 0.104 and 0.101 nm,[19] to which the 4f orbital of Ce(III) contributes but a little. Conditions in the excited-state are very different, however, because of the large orbital radius of the Ce 5d electron, which is absent in La(III). Upon relaxation to equilibrium geometry of the excited 5d state, this distance will expand to the new equilibrium d(Ce 5d−OH). Contributions to the Stokes shift stem from stabilization of the excited 5d state, $-\Delta V_{exc} \approx \frac{1}{2}k_{exc}[d(\text{Ce 5d}-\text{OH}) - d(\text{Ce 4f}-\text{OH})]^2$ and an increased energy of the ground state upon the Franck–Condon down-transition, $\Delta V_{grnd} \approx + \frac{1}{2}k_{grnd}[d(\text{Ce 5d}-\text{OH}) - d(\text{Ce 4f}-\text{OH})]^2$, both represented within the harmonic approximation for the sake of a semiquantitative argument. The change in the ground-state energy will be the larger of the two contributions because of the higher frequency and shorter Ce−OH distance. The fundamental frequency of the stretching Ce−OH mode was estimated

(18) (a) Lindner, R.; Reichling, M.; Matthias, E.; Johansen, H. *Appl. Phys.* **1999**, *B68*, 233. (b) Radzhabov, E.; Kurobori, T *J. Phys.: Condens. Matter* **2004**, *16*, 1871.
(19) Shannon, D. *Acta Crystallogr., Sect. A* **1976**, *32*, 751.

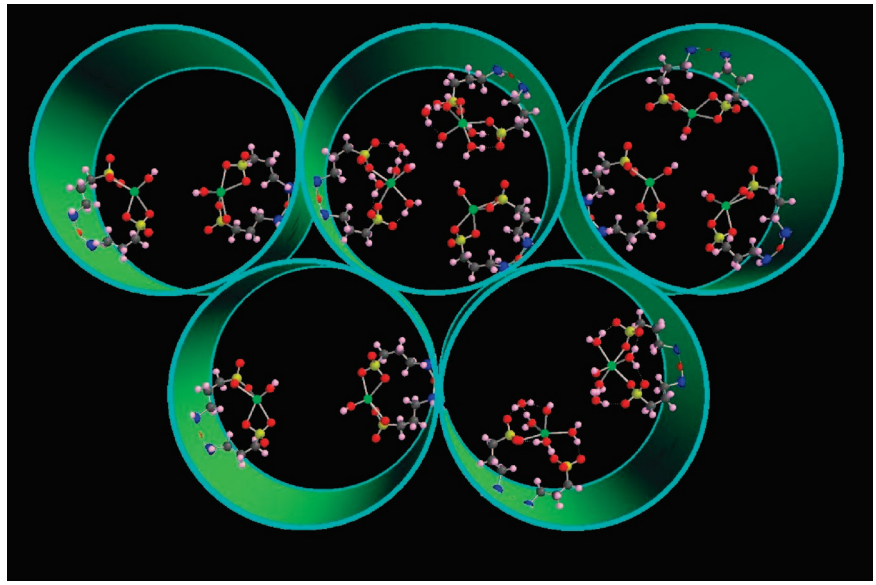

Figure 6. Pendant alkyl-sulfonic complexes of rare earth (RE) ions in the SBA material. For a pore diameter of ~7 nm, the molecular complexes, ca. 1 nm, are shown approximately twice their size in the mesopores. Color coding: green, trivalent RE ion; red, O; yellow, S; grey-black, C; pink, H; blue, Si. The upper left pore contains dehydrated monohydroxylated species optimized for RE = La(III) as in the Supporting Information, the lower right pore contains two tetra-aquo-hydroxylated species representing the hydrated complex optimized for La(III) as in the Supporting Information, and the remaining pores show the same two species in various proportions.

from all-electron DFT full-potential linearized augmented plane wave (FP-LAPW) calculations using the Wien2k code (see the Supporting Information), yielding the force constant $k_{grnd} = 554$ N m^{-1} on the basis of an estimate of the reduced mass of this linear oscillator, 0.015 kg/mol to yield the harmonic frequency 797 cm^{-1}. The experimental Stokes shift of 1.98 eV can be accounted for by an expansion $\Delta_{dist} = d$(Ce 5d−OH) − d(Ce 4f−OH) = 0.04 nm for ΔV_{grnd} alone.

The optimized structures, vibrational frequencies, and force constants are quite similar for the Ce(III) and La(III) complexes, mainly because the RE−OH bonding is primarily ionic and the RE−OH vibrational mode is localized. The optimized structures also do not depend on whether the calculation is DFT-FPLAPW as in the Wien2k platform or DFT-MOLCAO in the WF platform (see the Supporting Information). For example, a comparable frequency of the stretching La···OH mode based on DFT-MOLCAO calculations, 605 cm^{-1}, yields a force constant $k_{grnd} = 319$ N m^{1-} using the same reduced mass 0.015 kg/mol (see the Supporting Information). Thus, it is feasible to model the structure and vibrational modes using La(III) with an empty 4f shell to predict structure and vibrational modes of similar Ce(III) complexes with one additional electron in the 4f shell. This result will prove useful for the entire rare-earth series in which only small structural variations of low-symmetry RE(III) complexes need to be taken into account.

A very similar result is obtained by calculation of difluorolanthanum hydroxide, F_2LaOH, for which d(La−OH) = 0.219 nm and the calculated fundamental frequency of the stretching La···OH mode, 591 cm^{-1}, yields a force constant $k_{grnd} = 299$ N m^{1-}, using the reduced mass of 0.015 kg/mol. Both the distance and frequency of La−OH are again assumed to be close to the ground state of F_2Ce 4f−OH. Assuming $\Delta_{dist} = 0.045$ nm obtained above, the difluoro complex would give rise to a Stokes shift of 1.54 eV. Thus the replacement of two sulfonic groups by fluorides would yield a Stokes shift of a similar magnitude for both structures. Additional smaller effects of ΔV_{exc} can be estimated from calculated vibrational frequencies of the first excited electronic state of F_2La−OH, 100–200 cm^{-1}, and equilibrium distance d(La−OH) ≈ 0.26–0.28 nm for $k_{exc} \approx 9$ – 34 N m^{1-} and $-\Delta V_{exc} \approx 0.1$–0.2 eV. A contribution of $-\Delta V_{exc}$ will only add to this Stokes shift for the total, $\Delta V_{grnd} - \Delta V_{exc} \approx 1.6$–1.7 eV.

It remains to address the relation between the excitation energy of Ce(III)SBA on the basis of the excitation wavelength of 242 nm and the energy difference between the relevant ground and the excited states of the Ce(III) free ion. The excitation in Ce(III)SBA thus requires energy input of 5.12 eV. This is compared with the free-ion values for the difference between the lowest excited $^2D_{3/2}$ and the ground $^2F_{5/2}$ states of the Ce(III) ion, 6.17 eV.[20] The difference between the free Ce(III) ion and its SBA complex is interpreted in terms of bonding effects between the Ce(III) 5d orbitals of the excited state and the O 2p lone pairs particularly of the hydroxyl ligand, effects that are absent in the ground-state Ce(III) 4f. The 5d stabilization amounts to 1.17 eV. Additional effects are due to crystal-field splitting of the 5d levels, and all combined are consistent with the general classification due to van Krevel et al.[21] as (a) a shift in the center of gravity toward lower energies upon coordination to less electronegative ligands L that increase the covalency of the RE−L bond, and (b) an increase in ligand-field splitting of the RE 5d band with higher formal charge of L. The order of electronegativities of ligands considered here is F^- (4.1) > $-SO_3^-$ (3.23) > OH^- (2.85) > OH_2 (2.63), on the basis of estimates for the multielement groups

(20) National Institute of Standards and Technology Atomic Spectra Database, http://physics.nist.gov.

(21) Krevel, J. W. H van; Rutten, J. W. T. van; Mandal, H.; Hinzen, H. T.; Metselaar, R. *J. Solid State Chem.* **2002**, *165*, 19.

using the Moser−Pearson rules.[22] Hence lowering of the 5d center of gravity and concomitant reduction of Stokes shift by the van Krevel rule (a) is expected to be in the opposite order, larger for hydroxyl than the holding sulfonic groups. The effects of ligand-field splitting (b) are more difficult to assess because of the low symmetry of the Ce complexes, but may be expected common to all through the interaction of the $5d_{z2}$ orbital symmetry-adapted in the direction of the linear Ce−OH bond. Thus the ligand-field effects would add a common shift further lowering the center of gravity of the 5d band.

Hydrated Ce(III)SBA. Optimized structures of hydrated Ce(III)−OH species were calculated on the model La complex in which four water molecules were added to yield the stoichiometry $(H_2Si)_2O[(CH_2)_3SO_3]_2LaOH\cdot 4H_2O$ with three water molecules directly coordinated to the rare-earth ion to form a hexacoordinated complex and one additional outer-sphere water molecule making a hydrogen-bonded network with the hydroxyl, directly coordinated water ligands, and one of the sulfonate groups (see the Supporting Information). On the basis of the agreement between structures optimized by the DFT-FPLAPW and DFT-MOLCAO methods for the water-free Ce(III)SBA, we employed the latter method using La(III) for this complex. The main effect of the coordinated water is to increase the La−OH distance from 0.219 to 0.226 nm and lower the La−OH vibrational frequency from 605 to 503 cm^{-1}, for the force constant $k_{grnd} = 220$ N m^{1-}. This lowering of the vibrational frequency of the shortest La−O bond is mainly due to the bonding of the outer-sphere water molecule hydrogen down to the oxygen of the hydroxyl. Experimental Stokes shifts for the hydrated Ce(III)SBA-60 can be gleaned from data in Figure 4. The two broad excitation bands with maxima at 251 and 296 nm that excite the emission at 368 nm amount to Stokes shifts of 1.57 and 0.82 eV. In particular, the observed Stokes shift of 0.82 eV is substantially smaller than that in the dehydrated Ce−SBA material, 1.98 eV, simply because the ground-state potential energy well is shallower and the expanded excited state (Ce 5d−OH)$(H_2O)_x$ decays to a (Ce 4f−OH)$(H_2O)_x$ ground-state in which the energy penalty associated with the expanded geometry is smaller than in the dehydrated Ce(III)SBA-350 material. In semiquantitative terms, the Stokes shift of 0.82 eV would be accounted for by an expansion of 0.0345 nm, whereas a 1.57 eV shift would require an expansion of 0.0477 nm. Because the latter value is close to that of the dehydrated material, the Ce(III)SBA-60 material is considered to be a mixture of partially hydrated and fully hydrated structures giving rise to larger and smaller Stokes shifts. From relative intensities, it is further apparent that the partially hydrated fraction excited with 251 nm affords a greater efficiency of the luminescence than the fully hydrated fraction excited with the longer wavelength of 295 nm.

The simple direct mechanism is also supported by the similarity of the emissions of the present hydrated Ce(III)SBA-60 with that of aqueous solution of $Ce(III)Cl_3$ characterized by the following parameters: λ(emission) = 368 nm, λ(excitation of the 368 nm emission) = 230(w), 280(s), and 295(s) nm. Here, because of the high concentration of water, the long-wavelength excitations dominate. Because the silica matrix is absent in the Ce(III)(aq) solution and the luminescence parameters are similar to the Ce(III) complexes exchanged into the SBA material, and further, because these complexes are isolated from the silica support by the propyl-sulfonic spacers, the role of the silica matrix of SBA in excitation energy transfer of the multistep model appears unlikely. A comparison of the luminescence spectra in the present Ce(III)SBA materials, Ce(III) in Ce(IV)-impregnated mesoporous silica of Cai et al.,[10] and Ce(III)(aq) shown in Figure 5 demonstrates the similarities of the Ce(III) luminescence that can all be accounted for by the simple direct model on the basis of the large Stokes shift because of relaxation of the compressed to equilibrium Ce 5d complexes in which subtle differences in local vibrational modes and crystal-field effects give rise to structure-sensitive shifts and differences in excitation spectra.

Even with the short luminescence lifetimes in the 10 ns range,[18] the 5d → 4f emission will occur from completely structurally relaxed Ce 5d state: for example, the 605 cm^{-1} vibrational mode (see the Supporting Information) will traverse the distance of 0.05 nm from the compressed to the relaxed structure in picoseconds, whereas the luminescence lifetimes are nanoseconds. A further detail is apparent from the asymmetric shape of the 5d → 4f emission, which is resolved to two components separated by 0.13 eV in aqueous solution, 0.15 eV in room-temperature-dried Ce(III)SBA (aq, 0.16 eV in Ce(III)SBA-60, and 0.25 eV in Ce(III)SBA-350. These numbers are smaller than but comparable to the atomic splitting of the spin–orbit coupled 4f states $^2F_{7/2}$ and the lowest term $^2F_{5/2}$, 0.28 eV.[20]

Conclusions

The SBA materials derivatized with propyl-sulfonic groups to monovalent ion-exchange capacity of ∼1 meq/g are exchanged with Ce(III) to ∼0.5 meq/g to form a Ce(III)SBA material that displays a high-intensity purple photoluminescence. XPS and NIR-DRS analysis suggests a monohydroxylated Ce(III) bound to two proximal propyl-sulfonate groups in a complex $[\equiv Si\text{-}(CH_2)_3SO_3]_2Ce(III)OH\cdot xH_2O$, where x can be reduced to $\ll 1$ upon anoxic dehydration at 350 °C. The XPS reveals the Ce(III) 4f electron above the top of the valence band, thus identifying Ce(III) 4f as the HOMO. Photoluminescence emission and excitation spectra of the 5d → 4f emission show Stokes shifts and structure sensitivity consistent with a direct transition process not involving, in these SBA materials, a multistep energy transfer previously invoked for oxide phosphors. In the direct model, a local Franck–Condon transition 4f → 5d is followed by a relaxation of the Ce−OH bond due to the excited 5d orbitals being roughly twice the size the ground state 4f before photoemission takes place. A quantitative assessment of the relaxation and associated Stokes shifts is made on the basis of calculation of the vibrational frequency of excited states of RE−OH complexes.

(22) (a) Moser, E.; Pearson, W. P. *Helv. Phys. Acta* **1957**, *30*, 222; (b) Gibson, A. F. *Progress in Semiconductors*; Heywood & Co. Ltd.: London 1960, p 103.

A summary graphic representation of the intraporous pendant complexes is shown in Figure 6, which also illustrates the potential of multiple cation substitution with ensuing control of optical properties using various rare-earth emitters of different colors and energy transfer from one rare-earth complex to another for optical communication.

Acknowledgment. We gratefully acknowledge the support of this work by the U.S. Department of Energy (DE-FG02-01ER15181), the Pool Foundation for an undergraduate grant to L.L.Z., and a U.S. Army Grant to M.K.H. for the XPS analyses.

Supporting Information Available: LAPW calculations, geometry optimizations, vibrational frequencies and table of equlibrium bond distances (PDF). This material is available free of charge via the Internet at http://pubs.acs.org.

CM071754G